Journal Pre-proof

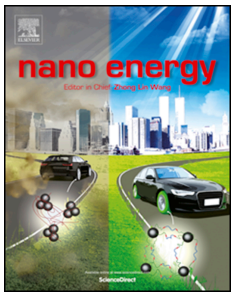

Piezotronic Spin and Valley Transistors Based on Monolayer MoS_2

Ruhao Liu, Gongwei Hu, Minjiang Dan, Yaming Zhang, Lijie Li, Yan Zhang

PII: S2211-2855(20)30235-4

DOI: https://doi.org/10.1016/j.nanoen.2020.104678

Reference: NANOEN 104678

To appear in: *Nano Energy*

Received Date: 31 January 2020

Revised Date: 3 March 2020

Accepted Date: 5 March 2020

Please cite this article as: R. Liu, G. Hu, M. Dan, Y. Zhang, L. Li, Y. Zhang, Piezotronic Spin and Valley Transistors Based on Monolayer MoS_2, *Nano Energy*, https://doi.org/10.1016/j.nanoen.2020.104678.

TOC Graphic

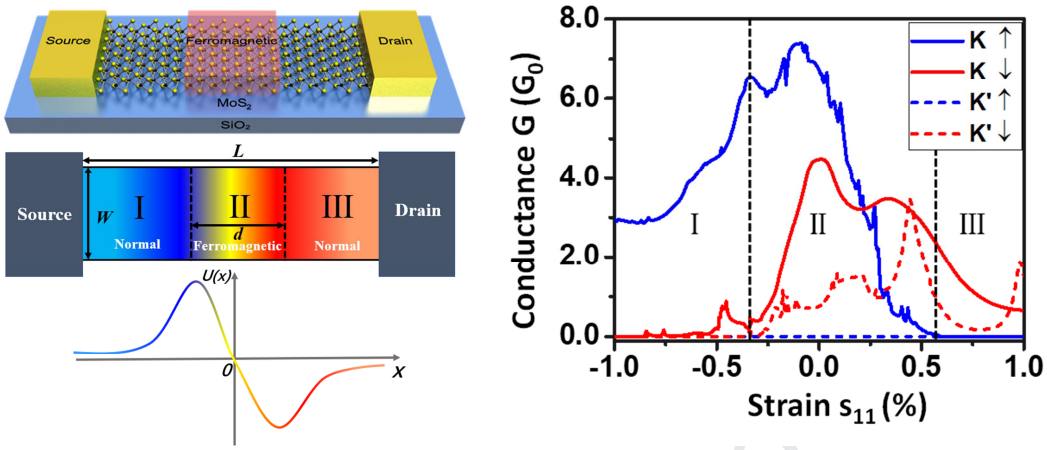

Piezotronic effect on monolayer MoS_2 has been investigated based on a normal-ferromagnetic-normal structure. The piezoelectric field at the interface of two-dimensional materials can modulate quantum transport by applied strain, which can effectively control spin and valley polarization. The quantum piezotronic transistor can act as a block unit of spin and valley filters for quantum information and storage.

Piezotronic Spin and Valley Transistors Based on Monolayer MoS_2

Ruhao Liu [1, †], Gongwei Hu [1, †], Minjiang Dan [1], Yaming Zhang [1], Lijie Li [2,*] and Yan Zhang[1,3,*]

[1] *School of Physics, University of Electronic Science and Technology of China, Chengdu 610054, China*

[2] *Multidisciplinary Nanotechnology Centre, College of Engineering, Swansea University, Swansea, SA1 8EN, UK*

[3] *Beijing Institute of Nanoenergy and Nanosystems, Chinese Academy of Sciences; National Center for Nanoscience and Technology (NCNST), Beijing 100083, China*

[†]This author contributes equally to this work.

[*]To whom correspondence should be addressed, E-mail: zhangyan@uestc.edu.cn and L.Li@swansea.ac.uk

Abstract

Piezotronics and piezo-phototronics based on the third generation semiconductors are two novel fields for low power consumption, self-powered technology and internet of things. Strain-induced piezoelectric field plays a key role to modulate not only charge-carrier transport but also quantum transport properties in piezoelectric semiconductors, especially for two-dimensional materials which can withstand large strain. In this paper, we theoretically study piezotronic effect on the modulation of spin and valley properties in single-layered MoS_2. Spin- and valley-dependent conductance, electronic density distribution and polarization ratio are investigated by quantum transport calculation. Because of piezotronic effect, strain-gated spin and valley transistors have excellent quantum state selectivity using by strain. Our work provides not only piezotronic effect on spin and valley quantum states, but also a guidance for designing novel quantum piezotronic devices.

Keywords: piezotronics, quantum transport, monolayer MoS_2

1. Introduction

Piezotronics and piezo-phototronics are two emerging fields which can be used for self-powered systems, flexible electronic devices, and human-computer interface [1-3]. Owing to coupling characteristics of piezoelectricity, semiconductor and photoexcitation, piezotronic and piezo-phototronic effect can be used to control electronic transport and optical excitation process by strain-induced polarized charges [4-7]. A variety of high performance piezotronic devices such as nanogenerators [8], flexible piezotronic strain sensors [9], piezotronic logic nanodevices [10], photoluminescence devices [11] have been developed based on piezoelectric semiconductors materials, such as ZnO, GaN and monolayer MoS_2 [12]. Recently, piezotronic effect on quantum materials has been studied theoretically, and piezo topological insulator devices have ultrahigh ON/OFF ratio and low power consumption [13-15].

Transition-metal dichalcogenides (TMDs) have been paid much attention in both fundamental physics and practical devices applications [16, 17]. The quantum spin Hall effect is found in WSe_2 [17]. Quantum wells based on two-dimensional (2D) layer-structured TMDs have unique optical features of intersubband transition [18]. The symmetry and strong spin-orbit coupling of TMDs can obtain spin and valley polarization [19, 20]. Valley is a local extremum point of the Bloch. For example, valley is a local maximum in the valence band, or local minimum in the conduction, and can be used to design new quantum devices as an internal quantum degree of freedom due to breaking center inversion symmetry [20], such as reversible valley NAND gate, valley filter and valley valve [21, 22]. Spin and valley quantum devices are good candidates for quantum information process and storage [23], for example, a valley sensitively response to different polarization of light due to the strong valley-light coupling [24].

Single quantum state of spin or valley need ultra-high electric field in 2D materials [25-28], which is a great challenge [26]. Gate voltage provides an electric field intensity of 100 kV/cm [29, 30]. It is very difficult to further increase the electric field. Using MoS_2

transistor with gate length of 1 nm, electric field can reach up to 1 MV/cm [31]. There are ultra-high electric field in piezoelectric semiconductor quantum wells, which can reach over 10 MV/cm [29, 32]. Ultra-high electric field will offer unique modulation for quantum devices, which is important for quantum piezotronics.

In this paper, a piezotronic normal-ferromagnetic-normal monolayer MoS_2 is studied theoretically. The ferromagnetic material in the middle structure can magnetize MoS_2 and bring in an exchange field under the magnetic field [33]. Transport characteristics of spin and valley is controlled by strain, which is superior to the gate voltage control mode [34]. This work paved a new way to the control of the spin and valley by piezotronic effect.

2. Theoretical Model of Piezotronic Effect on Quantum Transport

Take monolayer MoS_2 piezotronic transistor as an example, we use normal-ferromagnetic-normal MoS_2 junction. The ferromagnetic region with the exchange field connects to the two normal MoS_2 regions in the monolayer MoS_2 transistor, as shown in Figure 1(a). The ratio of piezoelectric coefficient to relative permittivity of MoS_2 is ~ 18 pC/m, higher than $MoSe_2$, WS_2 and WSe_2 (16, 15 and 12 pC/m). MoS_2 has been successfully synthesized to integrate into ferromagnetic materials [35]. The model can be used for other two-dimensional materials, such as $MoSe_2$, WS_2 and WSe_2. Spin- and valley-dependent quantum transport properties can be obtained from the Schrödinger equation

$$H\psi = E\psi \tag{1}$$

where H donates a Hamiltonian, ψ stands for wave function and E is eigenvalue. The main transport properties including the transmission conductance and electronic density distribution can be obtained by solving the Schrödinger equation under special boundary condition.

Spin and valley polarization can be obtained in a normal-ferromagnetic-normal junction based on 2D materials applying a high intensity magnetic field [36]. The model can be described by the Hamiltonian [20, 34, 37]

$$H = \hbar v\left(\tau_z k_x \sigma_x + k_y \sigma_y\right) + \Delta\sigma_z + (-\lambda\tau_z s_z \sigma_z + \lambda\tau_z s_z) - s_z h + U \tag{2}$$

where τ_z =±1 donates the valleys index (1 for **K** valley and -1 for **K'** valley), s_z =±1

represents the electron spin up and spin down. σ is the Pauli matrices. k_x and k_y are the wave vector momentum. Δ is the energy gap. λ is the spin splitting energy of the valence band and v is the Fermi velocity. h is the exchange field existing in the ferromagnetic region and U is the externally applied electric potential.

While a uniform strain is applied on MoS_2, strain-induced piezoelectric charges at the two boundaries generate piezoelectric field, which can be considered approximately as an one-dimensional field [38]. The direction of monolayer MoS_2 is shown in Figure 1(a) where armchair direction is electronic transport from source to drain. The strain is applied along armchair direction, and piezoelectric charges are induced at the zigzag interfaces due to nonzero piezoelectric coefficient e_{11}. The piezoelectric charges has been reported in MoS_2 based nanogenerators [39]. The piezoelectric potential inside the materials can be written as [40]:

$$U_{piezo}=\begin{cases}\dfrac{e_{11}s_{11}}{2\pi\varepsilon_r\varepsilon_0}\ln|x|+U_1, -d<x\le 0\\ \dfrac{e_{11}s_{11}}{2\pi\varepsilon_r\varepsilon_0}\ln\left|\dfrac{x}{d-x}\right|, 0<x\le d\\ \dfrac{e_{11}s_{11}}{2\pi\varepsilon_r\varepsilon_0}\ln|x-d|+U_2, d\le x<2d\end{cases} \tag{3}$$

where e_{11} is the piezoelectric constant, s_{11} is the applied strain, ε_r is relative dielectric constant, ε_0 is vacuum permittivity, x is the distance away from the boundary and d is the width of the ferromagnetic region. In order to ensure that the electric potential is equal at different regional interfaces and the logarithmic function is meaningful, we set the corresponding parameters, which are represented by constants U_1 and U_2, respectively. The piezoelectric field and piezopotential inside the heterojunction is shown in Figure 1(b) under an external strain -1%. Due to large piezoelectricity for monolayer MoS_2, piezoelectric charges are generated at two interfaces between normal and ferromagnetic region. The positive and negative piezoelectric charges can be served as an electric dipole, and its electric field distribution is shown in Figure 1(b). For this piezoelectric dipole, piezoelectric field is very strong with order of MV/cm near piezoelectric charges (or interfaces) but becomes weak away from the charges (or interfaces). It should be noted that direction of piezoelectric field is

positive in ferromagnetic region but negative in two normal regions, which is a typical feature of electric dipole. The localization of piezoelectric field induces an antisymmetric distribution of piezoelectric potential that can effectively control spin and valley transport.

In the normal-ferromagnetic-normal structure, the wave function is divided into three parts, the left lead, the ferromagnetic strip, and the right lead [41], which can be written as

$$\begin{aligned}\Psi^L &= e^{ik^L_{m'}(x-x_0^L)}\sum_n \chi^L_{m',n}\varphi_n(y)+\sum_{mn} b^L_m \chi'^L_{m,n} e^{ik'^L_m(x-x_0^L)}\varphi_n(y)\\ \Psi^F &= \sum_{mn} a^F_m \chi^F_{m,n} e^{ik^F_m(x-x_0^F)}\varphi_n(y)+\sum_{mn} b^F_m \chi'^F_{m,n} e^{ik'^F_m(x-x_0^F)}\varphi_n(y)\\ \Psi^R &= \sum_{mn} a^R_m \chi^R_{m,n} e^{ik^R_m(x-x_0^R)}\varphi_n(y)\end{aligned} \tag{4}$$

k_m and k'_m are the wave vectors in the left lead and right lead respectively. $k_{m'}$ represents wave vectors in a given subband m' in the left lead, $k'_{m'}$ is the same in the right lead. a_m and b_m donate the coefficients of the scattering matrix while χ stands for the expanded coefficients. We can calculate the coefficients in each strip by using scattering matrix theory. Therefore, the density distribution of the electron $|\Psi(x,y)|^2$ and the total conductance can be obtained by the Landauer-Buttiker formula [36],

$$G_{\tau s} = G_0 \sum_{mn} \left| t^{\tau s}_{mn} \right|^2 \tag{5}$$

where $t^{\tau s}_{mn}$ is the valley (τ) and spin (s) dependent scattering coefficient from the *m*-th incoming mode to the *n*-th outcoming mode. $G_0 = e^2/h$ is the conductance unit.

We then obtain valley- and spin-dependent conductance by using $G_{\mathbf{K}} = \left(G_{\mathbf{K}\uparrow} + G_{\mathbf{K}\downarrow}\right)/2$, $G_{\mathbf{s}} = \left(G_{\mathbf{Ks}} + G_{\mathbf{K's}}\right)/2$. The capability of valley and spin filtering can be characterized by the degree of valley and spin polarization [36], defined as P_v and P_s

$$P_v = \frac{G_{\mathbf{K}} - G_{\mathbf{K'}}}{G_{\mathbf{K}} + G_{\mathbf{K'}}} \tag{6}$$

$$P_{\mathbf{s}} = \frac{G_{\mathbf{K}\uparrow} + G_{\mathbf{K'}\uparrow} - G_{\mathbf{K}\downarrow} - G_{\mathbf{K'}\downarrow}}{G_{\mathbf{K}\uparrow} + G_{\mathbf{K'}\uparrow} + G_{\mathbf{K}\downarrow} + G_{\mathbf{K'}\downarrow}} \tag{7}$$

Valley magnetoelectricity effect, the phenomenon of inducing a valley-dependent magnetization by piezoelectric field, has recently been observed in monolayer MoS_2 when a

current flows in a piezoelectric field. According to the theoretical analysis [42], the current perpendicular to strain-induced piezoelectric field can produce an out-of-plane magnetization, following the relationship $\mathbf{M}_V \sim \mathbf{E}_{pz} \times \mathbf{J}$ with net valley magnetization $\mathbf{M}_V$, piezoelectric field $\mathbf{E}_{pz}$ and current $\mathbf{J}$. Piezoelectric field is parallel to source-drain current, as shown in Figure 1. Therefore, valley magnetization is neglected in this study.

3. Results and Discussion

To compute the transport properties, we use the quantum transport package KWANT which is based on the wave function method. This approach is mathematically equivalent to the commonly used nonequilibrium Green's function [43]. Owing to size effect, electronic transport properties depend on the strip length and width [44, 45]. According to typical normal-ferromagnetic-normal structure [46], we assume that the strip width is 40 nm and the length is 140 nm while the width of the ferromagnetic region is 20 nm. In this size, the piezoelectric potential is same order of magnitude with the energy intervals between subbands. The Fermi velocity $v = 5.3 \times 10^5$ m·s^{-1}, the spin splitting λ =37.5 meV and band gap Δ =833 meV [34, 37].

The strain distribution is uniform and strain-induced piezoelectric potential is symmetrical. The elastic modulus of middle layer of ferromagnetic material is ~ 200 GPa (EuO and EuS), and polyethylene terephthalate (PET) is < 100 MPa. [47, 48]. When substrate is bent with a small strain, the piezoelectric charges are located at interface between normal and ferromagnetic monolayer MoS_2.

In this paper, we study spin and valley conductance with various strain by quantum transport calculation. Figure 2(a) shows optimized Fermi level of -0.98 eV, which indicate spin polarization. In experimental, Fermi level is accurately controlled by means of material doping or substrate gate voltage [49, 50]. Figure 2 shows the results for valley and spin conductance as a function of strain under Fermi level of -0.98eV. The blue curves donate the spin up conductance while the red curves represent the spin down conductance. The solid curves are the **K** valley conductance and the dashed lines correspond to **K′** valley conductance. As strain varies from -1.0% to 1.0%, there are three regions of conductance distribution. In the left region *A*, strain ranges from -1.0% to -0.3%. It shows the electrons in

K valley has high conductance but near zero conductance in **K′** valley. In this case, both spin up and spin down electrons in **K** valley can be effectively selected by external strain. The electrons in **K′** valley are filtered out. In this way, the charge current is fully valley polarized in the left region. In the middle region *B*, the total conductance of **K** valley (solid line) is greater than **K′** valley (dashed line) with various strain from -0.3% to 0.6%. It is obviously that the flowing current is mainly contributed from **K** valley electrons. In this way, the middle region shows the incomplete valley polarization, which is result from the imbalance of the conductance contribution from **K** and **K′** valley. In the right region *C*, a fully spin-polarized conductance is obtained while strain increases from 0.6% to 1.0%. The spin degeneracy of the conduction band edges can be eliminated by the exchange field. It is observed that spin-down electrons (red line) have nonzero conductance, exhibiting a good selectivity of spin electrons by external strain. The exchange field in F region have been studied in graphene, silicene and TMDs [36, 51]. Spin splitting can be induced by using the magnetic insulator EuO deposited on graphene [33]. Although previous works presents the valley filtering in graphene structures by strain control [27, 28], it is difficult to obtain valley and spin at the same time. In addition, previous works also need large magnetic field [52]. It maybe not suitable for low power consumption and miniaturization of the devices. The selectivity of spin and valley in their transport is the result of strong electric field produced by piezoelectric charges at the interface, which is piezotronic effect on quantum materials.

Figure 2(b) show the case of E_F = -0.9 eV, which is nonzero conductance for the **K'** valley and down spin electron. Figure 2(c) show the case of E_F = -1.0 eV, which is up spin polarization (blue solid and dashed) for strain from -1.0% to -0.25%. This polarization is mixed by **K** and **K'** valley conductance. For E_F = -1.1 eV case in Figure 3(d), there are two polarization regions where one is **K'** valley, up spin polarization at strain <-0.25%, and down spin polarization at strain > 0.75%.

Figure 3 displays the density distribution of spin up electrons in **K** valley. Strain is fixed at -0.2% and thus a steady potential distribution is produced. Different quantum states appear in the system. At Fermi energy of -1.19 eV, the electrons mainly reside in the middle of the ferromagnetic region while two normal MoS_2 regions have little electrons, as shown in Figure 3(a). This highly localized distribution of the electrons is due to the piezoelectric potential.

The potential well is in the ferromagnetic region, and potential barrier is in the two sides. When the electronic energy is higher than potential well and lower than barrier, the electronic wave function will oscillate at the well and damp rapidly at the barrier. The properties can also be found in GaAs and GaN quantum well [53]. As the Fermi level decreases to -1.20 eV, electronic channels in the left region is open. Some electrons are blocked before entering the left ferromagnetic region owing to the high piezoelectric potential barrier generated from the left ferromagnetic boundary. Owning to the quantum size effect, there are distinct transport modes and many quantum states, as shown in Figure 3(b) and 3(c). The electrons can be completely blocked by the piezoelectric potential barrier of the left ferromagnetic region in Figure 3(b). The electrons can also partially travel the barrier for some special channels by quantum tunneling effect, as shown in Figure 3(c). Figure 3(d) shows the decrease of electrons in the ferromagnetic region at Fermi energy of -1.21 eV. Although we take spin up electrons in **K** valley as an example, other spin and valley electrons show similar transport in this device.

Figure 3(e) is band dispersion with strip width of 10 and 40 nm. Figure 3(f) is the enlarged band dispersion. For improving controllability, energy interval between two subbands can be changed by device size. While the width of MoS_2 increase from 10 to 40 nm, energy interval between two subbands decrease from ~ 0.1 eV to ~ 0.01, as shown in Figure 3(f).

Although Figure 3(b) and 3(c) have a same EF = -1.20 eV, the different transport channels will induce various transport behaviors. When electronic momentum Kx is small, the electrons will oscillate along y direction. In Figure 3(b), oscillation is strong and the electrons will exhibit coupling [44, 45].

Figure 4 gives a full insight of piezotronic effect on the transport properties. The strain varies from -1.0% to 1.0% and Fermi level is set from -1.4 eV to -0.7 eV. The distribution of conductivity regions is corresponding to different valleys and spins. In **K** valley, spin up electrons exist a relatively high conductance, while Fermi level is fixed from -1.2 eV to -0.95 eV and strain is set from -1.0% to 0.5%, as shown in Figure 4(a), alternatively, spin down electrons exist a relatively high conductance when Fermi level is fixed from -1.4eV to -0.9eV and strain is set from -0.75% to 1.0%, as shown in Figure 4(b). In **K′** valley case, the conduct region of spin up electrons is concentrated on the bottom left of parameter plane when Fermi

energy is from -1.35 eV to -1.1 eV and strain is from -1.0% to 0.5%, as shown in Figure 4(c). Figure 4(d) shows the nonzero conductance region of spin down electrons at the upper right, while the Fermi energy is from -1.05 eV to -0.78 eV and the strain is applied from -0.75% to 1.0%. The spin and valley distribution give a clear guidance of the quantum state selection by piezotronic effect.

Figure 5 shows spin-polarized ratio P_s and valley-polarized ratio P_v, which are an effective parameter to describe the performance of filtering behavior for spin and valley transport properties. For spin-polarized case, there are two regions with highly polarized ratio, as shown in Figure 5(a). The blue region in the lower left corner shows a distinct spin-up selection while the red region in the upper right corner presents a clear spin down selection. The absolute value of spin-polarization ratio is close to 1, demonstrating the excellent selective behavior by externally applied strain. Strain can also effectively modulate valley polarization. For valley-polarized case, two separated regions of **K′** valley polarization and one region for **K** valley polarization is shown in Figure 5(b). The results reveal the potential of the proposed region for application in spin- and valley-based electronics.

Piezotronic MoS_2 transistors can server as block units of spin and valley filters. Figure 6(a) displays the experimental realization of the proposed spin and valley transistors. Monolayer MoS_2 is placed on a polyethylene terephthalate flexible substrate underneath which a thin electrode material Si is imposed for accurately tuning Fermi level. Ferromagnetic material EuO is placed on the middle of MoS_2 to induce exchange field, and source-drain electrodes are welded for providing transport voltage V_{ds}. By bending flexible substrate, strain can be applied to MoS_2 for modulating spin and valley transport.

When the current passes through the channel, spin and valley are regulated by the strain-induced piezoelectric field. Figure 6(b) shows the spin-polarized characteristics while the Fermi level in the spin up energy bands. The conduction current comes mainly from the contribution of the spin up state. Valley polarization selection is shown in the Figure 6(c). While the Fermi level is between the spin-up and spin down energy bands, spin selectivity by strain disappear, as shown in Figure 6(d). Similarly, the selectivity of the strain to the valley also disappears, as shown in Figure 6(e). Figure 6(f) and Figure 6(g) show the cases at the Fermi level in spin down band and K’ valley band, respectively. Corresponding to Figure 6(b)

and 6(c), there are the spin-down and K' valley polarization states.

4. Summary

In this study, piezotronic effect on electronic spin and valley transport properties have been studied by using a normal-ferromagnetic-normal monolayer MoS_2 transistor. The transport characteristics are significantly affected by the strain-induced strong piezoelectric field. Spin and valley polarization can be induced by strain. Spin and valley filters have novel selectivity of piezotronic spin and valley transistors, which have potential application in quantum information. This study provides a promising platform to develop novel quantum piezotronic devices.

Reference

1. Pan, C., J. Zhai, and Z.L. Wang, *Piezotronics and Piezo-phototronics of Third Generation Semiconductor Nanowires.* Chemical reviews, 2019. **119**(15): p. 9303-9359.
2. Wang, Z.L., W. Wu, and C. Falconi, *Piezotronics and piezo-phototronics with third-generation semiconductors.* MRS Bulletin, 2018. **43**(12): p. 922-927.
3. Wu, W. and Z.L. Wang, *Piezotronics and piezo-phototronics for adaptive electronics and optoelectronics.* Nature Reviews Materials, 2016. **1**(7): p. 16031.
4. Zhang, Y., Y. Liu, and Z.L. Wang, *Fundamental theory of piezotronics.* Adv Mater, 2011. **23**(27): p. 3004-13.
5. Zhang, Y., et al., *Theory of piezotronics and piezo-phototronics.* MRS Bulletin, 2018. **43**(12): p. 928-935.
6. Liu, Y., et al., *Piezotronics and piezo-phototronics in two-dimensional materials.* MRS Bulletin, 2018. **43**(12): p. 959-964.
7. Zhu, L. and Z.L. Wang, *Progress in piezotronics and piezo-phototronics of quantum materials.* Journal of Physics D: Applied Physics, 2019.
8. Wang, Z.L. and J. Song, *Piezoelectric nanogenerators based on zinc oxide nanowire arrays.* Science, 2006. **312**(5771): p. 242-6.
9. Zhou, J., et al., *Flexible piezotronic strain sensor.* Nano Lett, 2008. **8**(9): p. 3035-40.
10. Wu, W., Y. Wei, and Z.L. Wang, *Strain-gated piezotronic logic nanodevices.* Adv Mater, 2010. **22**(42): p. 4711-5.
11. Li, L. and Y. Zhang, *Controlling the luminescence of monolayer MoS2 based on the piezoelectric effect.* Nano Research, 2017. **10**(7): p. 2527-2534.
12. Wang, Z.L., *Progress in piezotronics and piezo-phototronics.* Adv Mater, 2012. **24**(34): p. 4632-46.
13. Hu, G., et al., *Piezotronic Transistor Based on Topological Insulators.* ACS Nano, 2018. **12**(1): p. 779-785.
14. Dan, M., et al., *High performance piezotronic logic nanodevices based on GaN/InN/GaN topological insulator.* Nano Energy, 2018. **50**: p. 544-551.
15. Guo, X., et al., *Quantum information memory based on reconfigurable topological insulators by piezotronic effect.* Nano Energy, 2019. **60**: p. 36-42.
16. Mak, K.F. and J. Shan, *Photonics and optoelectronics of 2D semiconductor transition metal dichalcogenides.* Nature Photonics, 2016. **10**(4): p. 216-226.
17. Wang, Q.H., et al., *Electronics and optoelectronics of two-dimensional transition metal dichalcogenides.* Nat Nanotechnol, 2012. **7**(11): p. 699-712.
18. Schmidt, P., et al., *Nano-imaging of intersubband transitions in van der Waals quantum wells.* Nat Nanotechnol, 2018. **13**(11): p. 1035-1041.
19. Xu, X., et al., *Spin and pseudospins in layered transition metal dichalcogenides.* Nature Physics, 2014. **10**(5): p. 343-350.
20. Xiao, D., et al., *Coupled spin and valley physics in monolayers of MoS2 and other group-VI dichalcogenides.* Phys Rev Lett, 2012. **108**(19): p. 196802.
21. Park, C., *Magnetoelectrically Controlled Valley Filter and Valley Valve in Bilayer Graphene.* Physical Review Applied, 2019. **11**(4).
22. Ang, Y.S., et al., *Valleytronics in merging Dirac cones: All-electric-controlled valley filter, valve, and universal reversible logic gate.* Physical Review B, 2017. **96**(24).
23. Schaibley, J.R., et al., *Valleytronics in 2D materials.* Nature Reviews Materials, 2016. **1**(11).

24. Mak, K.F., D. Xiao, and J. Shan, *Light–valley interactions in 2D semiconductors.* Nature Photonics, 2018. **12**(8): p. 451.
25. Son, Y.W., M.L. Cohen, and S.G. Louie, *Half-metallic graphene nanoribbons.* Nature, 2006. **444**(7117): p. 347-9.
26. Khoeini, F., K. Shakouri, and F.M. Peeters, *Peculiar half-metallic state in zigzag nanoribbons of MoS2: Spin filtering.* Physical Review B, 2016. **94**(12).
27. Milovanović, S.P. and F.M. Peeters, *Strain controlled valley filtering in multi-terminal graphene structures.* Applied Physics Letters, 2016. **109**(20): p. 203108.
28. Fujita, T., M.B.A. Jalil, and S.G. Tan, *Valley filter in strain engineered graphene.* Applied Physics Letters, 2010. **97**(4): p. 043508.
29. Miao, M.S., et al., *Polarization-driven topological insulator transition in a GaN/InN/GaN quantum well.* Phys Rev Lett, 2012. **109**(18): p. 186803.
30. Yang, W., K. Chang, and S.C. Zhang, *Intrinsic spin hall effect induced by quantum phase transition in HgCdTe quantum wells.* Phys Rev Lett, 2008. **100**(5): p. 056602.
31. Desai, S.B., et al., *MoS2 transistors with 1-nanometer gate lengths.* Science, 2016. **354**(6308): p. 99-102.
32. Zhang, D., et al., *Interface-induced topological insulator transition in GaAs/Ge/GaAs quantum wells.* Phys Rev Lett, 2013. **111**(15): p. 156402.
33. Haugen, H., D. Huertas-Hernando, and A. Brataas, *Spin transport in proximity-induced ferromagnetic graphene.* Physical Review B, 2008. **77**(11).
34. Li, H., et al., *Gate-Voltage-Controlled Spin and Valley Polarization Transport in a Normal/Ferromagnetic/Normal MoS2 Junction.* ACS applied materials & interfaces, 2014. **6**(3): p. 1759-1764.
35. Peng, B., et al., *Valley Polarization of Trions and Magnetoresistance in Heterostructures of MoS2 and Yttrium Iron Garnet.* ACS Nano, 2017. **11**(12): p. 12257-12265.
36. Yokoyama, T., *Controllable valley and spin transport in ferromagnetic silicene junctions.* Physical Review B, 2013. **87**(24).
37. Li, X., F. Zhang, and Q. Niu, *Unconventional quantum Hall effect and tunable spin hall effect in Dirac materials: application to an isolated MoS2 trilayer.* Phys Rev Lett, 2013. **110**(6): p. 066803.
38. Zhang, J., et al., *Band alignment of two-dimensional lateral heterostructures.* 2D Materials, 2016. **4**(1): p. 015038.
39. Wu, W., et al., *Piezoelectricity of single-atomic-layer MoS2 for energy conversion and piezotronics.* Nature, 2014. **514**(7523): p. 470-4.
40. Jackson, J.D., *Classical electrodynamics*. 2007: John Wiley & Sons.
41. Zhang, L.B., et al., *Electrical switching of the edge channel transport in HgTe quantum wells with an inverted band structure.* Physical Review B, 2011. **83**(8).
42. Lee, J., et al., *Valley magnetoelectricity in single-layer MoS2.* Nat Mater, 2017. **16**(9): p. 887-891.
43. Maugin, G.A., *Continuum mechanics of electromagnetic solids*. 2013: Elsevier.
44. Beenakker, C.W.J. and H. van Houten, *Quantum Transport in Semiconductor Nanostructures.* 1991. **44**: p. 1-228.
45. Nazarov Y V, N.Y., Blanter Y M., *Quantum transport: introduction to nanoscience*. 2009: Cambridge university press.
46. Saxena, R., A. Saha, and S. Rao, *Conductance, valley and spin polarizations, and tunneling magnetoresistance in ferromagnetic-normal-ferromagnetic junctions of silicene.* Physical Review B,

2015. **92**(24).

47. Wachter, P., *Chapter 19 Europium chalcogenides: EuO, EuS, EuSe and EuTe*. 1979. **2**: p. 507-574.
48. Wegener, M., W. Wirges, and R. Gerhard-Multhaupt, *Piezoelectric Polyethylene Terephthalate (PETP) Foams – Specifically Designed and Prepared Ferroelectret Films.* Advanced Engineering Materials, 2005. **7**(12): p. 1128-1131.
49. Ohta, T., et al., *Controlling the electronic structure of bilayer graphene.* Science, 2006. **313**(5789): p. 951-4.
50. Oostinga, J.B., et al., *Gate-induced insulating state in bilayer graphene devices.* Nat Mater, 2008. **7**(2): p. 151-7.
51. Adrian G. Swartz, P.M.O., † Yufeng Hao,‡ Rodney S. Ruoff,‡ and Roland K. Kawakami†,*, *Integration of the Ferromagnetic Insulator EuO onto Graphene.* ACS nano, 2012: p. 10063–10069.
52. Guinea, F., M.I. Katsnelson, and A.K. Geim, *Energy gaps and a zero-field quantum Hall effect in graphene by strain engineering.* Nature Physics, 2009. **6**(1): p. 30-33.
53. Dohrmann, S., et al., *Anomalous spin dephasing in (110) GaAs quantum wells: anisotropy and intersubband effects.* Phys Rev Lett, 2004. **93**(14): p. 147405.

Ruhao Liu received his B.S. in applied physics in the School of Physics at University of Electronic Science and Technology of China in 2018. He is currently a M.S. student in group of Prof. Yan Zhang at UESTC. His research focuses on the field of piezotronics and piezo-phototronics, especially quantum piezotronics.

Gongwei Hu received his B.S. degree (2014) from China Three Gorges University and M.S. degree in Theoretical Physics (2017) from Lanzhou University. He is currently pursuing the Ph.D degree under the guidance of Professor Yan Zhang in School of Physics in UESTC. His research focuses on the field of functional nanostructures and their physics.

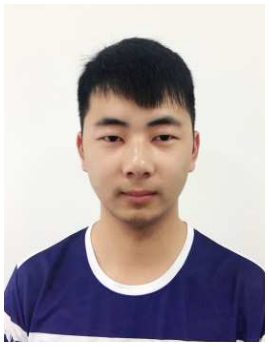

Minjiang Dan is currently pursuing his B.S. degree in the University of Electronic Science and Technology of China (UESTC). He is now simulating piezotronic devices under the guidance of Professor Yan Zhang in School of Physics. His interests focus on the quantum piezotronics, semiconductor device and solar cell.

Yaming Zhang received his B.S. in the School of Physics at University of Electronic Science and Technology of China in 2018. He is currently a M.S. student in group of Prof. Yan Zhang at UESTC. He is interested in new semiconductor nanodevices, and focuses on theory of piezotronics and piezophototronics.

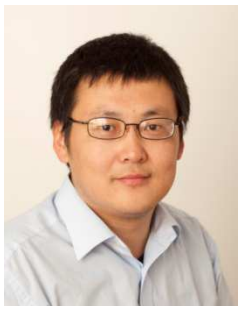

Lijie Li is a professor at Swansea University, UK. His research interests are design, modeling, fabrication, and characterization of MEMS, NEMS, sensors and actuators. He is Fellow of IET, and senior member of IEEE.

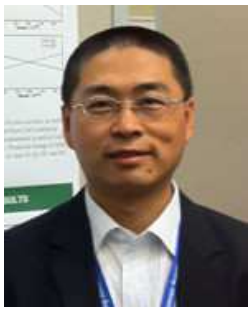

Yan Zhang is a professor at University of Electronic Science and Technology of China. He received his B. S. degree (1995) and Ph.D degree in Theoretical Physics (2004) from Lanzhou University. His research interests include self-powered nano/micro system, piezotronic and modeling of nonlinear dynamics of NEMS. He is senior member of IEEE.

Figure caption

Figure 1. (a) Schematic illustration of normal/ferromagnetic/normal monolayer MoS_2 junction device. The current direction is along armchair direction of MoS2. (b) Piezoelectric field and potential distribution under the strain $s_{11} = -1\%$. Strain distribution is uniform in two normal regions and zero in ferromagnetic region. Positive and negative interfacial piezoelectric charges form an electric dipole, and its field direction is also displayed.

Figure 2. Spin- and valley-dependent conductance against strain under the Fermi level of (a) -0.98 eV, (b) -0.90 eV, (c) -1.0 eV and (d) -1.1 eV. Only the conductance at E_F = -0.98 eV shows good polarization labelled as region *A* (spin up) and *C* (spin down). Region *B* is mixed by spin and valley conductance.

Figure 3. Density distribution of the up-spin electron in **K** valley at the Fermi level of (a) -1.19 eV, (b) -1.20 eV, (c) -1.20 eV, and (d) -1.21 eV. (e) The enlarged valence band dispersion of up-spin, **K**-valley electrons under the strip width of 10 nm (left) and 40 nm (right). (f) The enlarged band dispersion. Fermi levels at -1.19, -1.20 and -1.21 eV are displayed by different color dashed.

Figure 4. The distribution of planar conductance as a function of Fermi energy and strain. The left column (a, c) is for spin-up electrons, the right column (b, d) donates the spin-down electrons while the first row represents the **K** valley and the second row refers to the **K′** valley.

Figure 5. Contour plots of (a) spin polarized conductance G_s and (b) valley polarized conductance G_v as functions of Fermi energy and strain.

Figure 6. (a) Device diagram of spin-valley transistors. (b)-(g) Schematic diagram of strain and Fermi level regulating electron transport. The column on the left (b d, f) shows the process of the selection of spin polarization influenced by Fermi energy and strain. The right column (c, e, g) shows the screening procedure of the valley result from the changing of Fermi level and strain. Here the orange solid ball represents spin up while the blue solid one donates spin down. As for the hollow circle, the blue left arrow refers to **K** valley while the orange right arrow stands for **K′** valley.

Figure

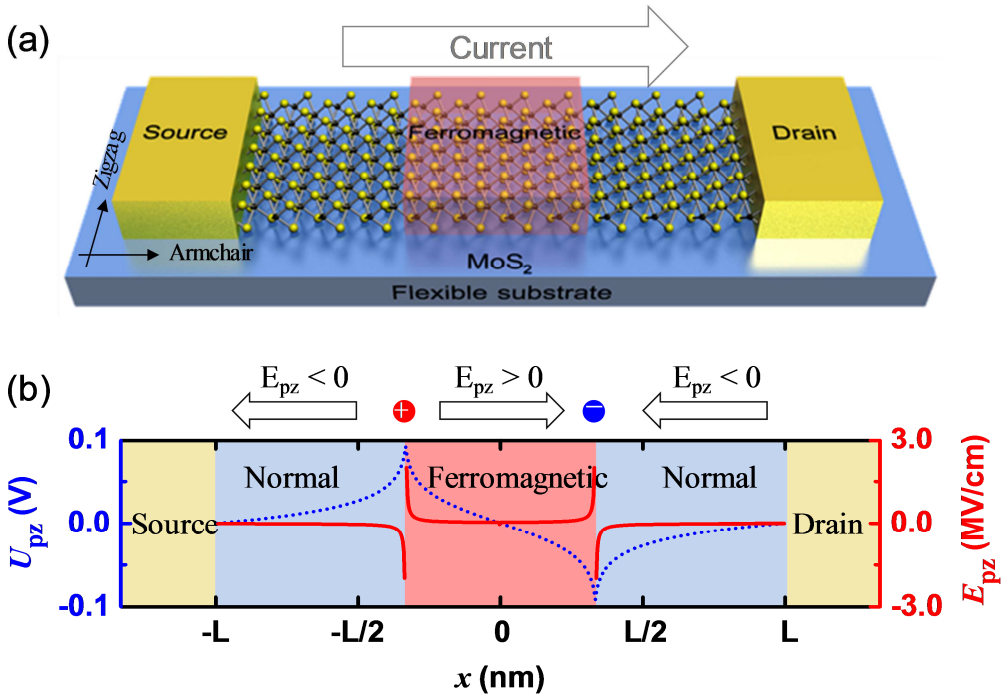

Figure 1

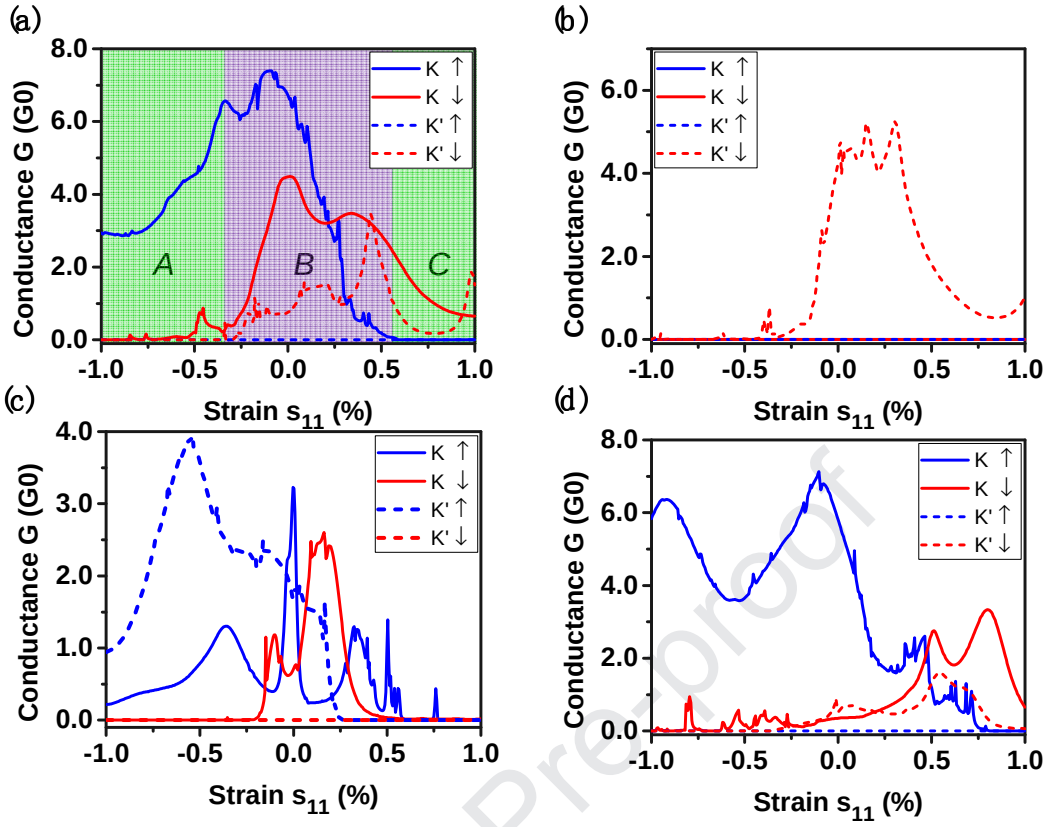

Figure 2

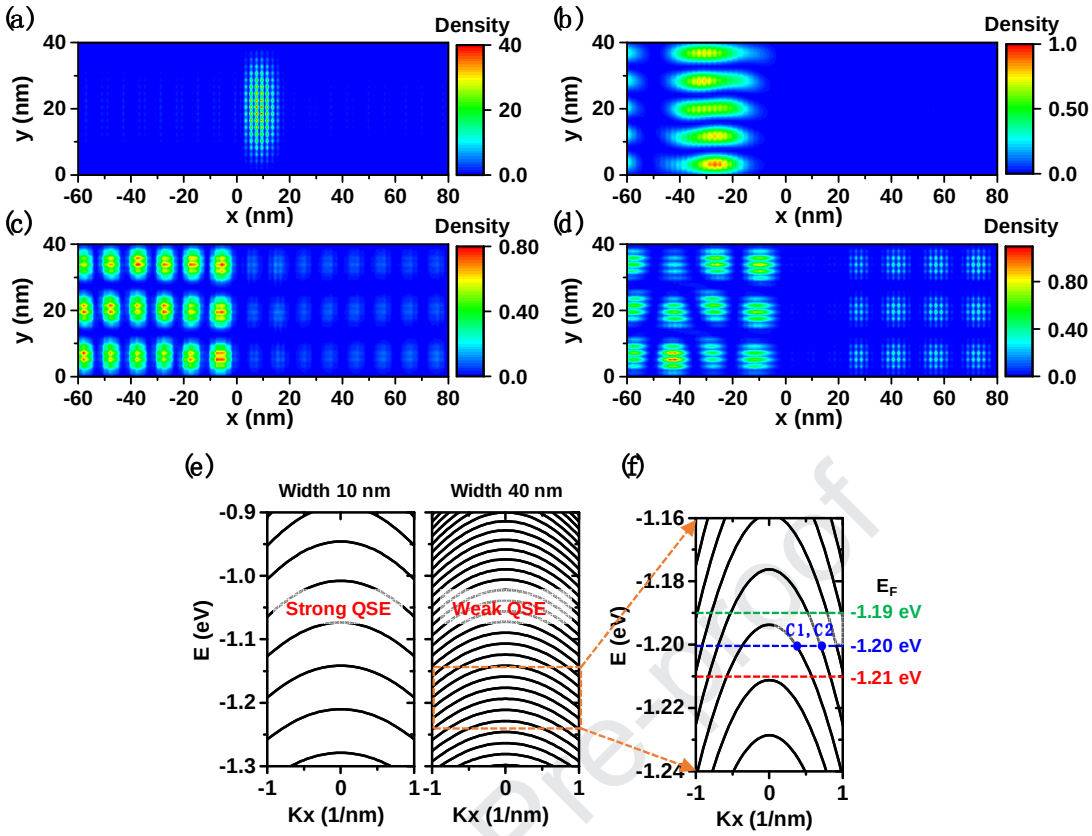

Figure 3

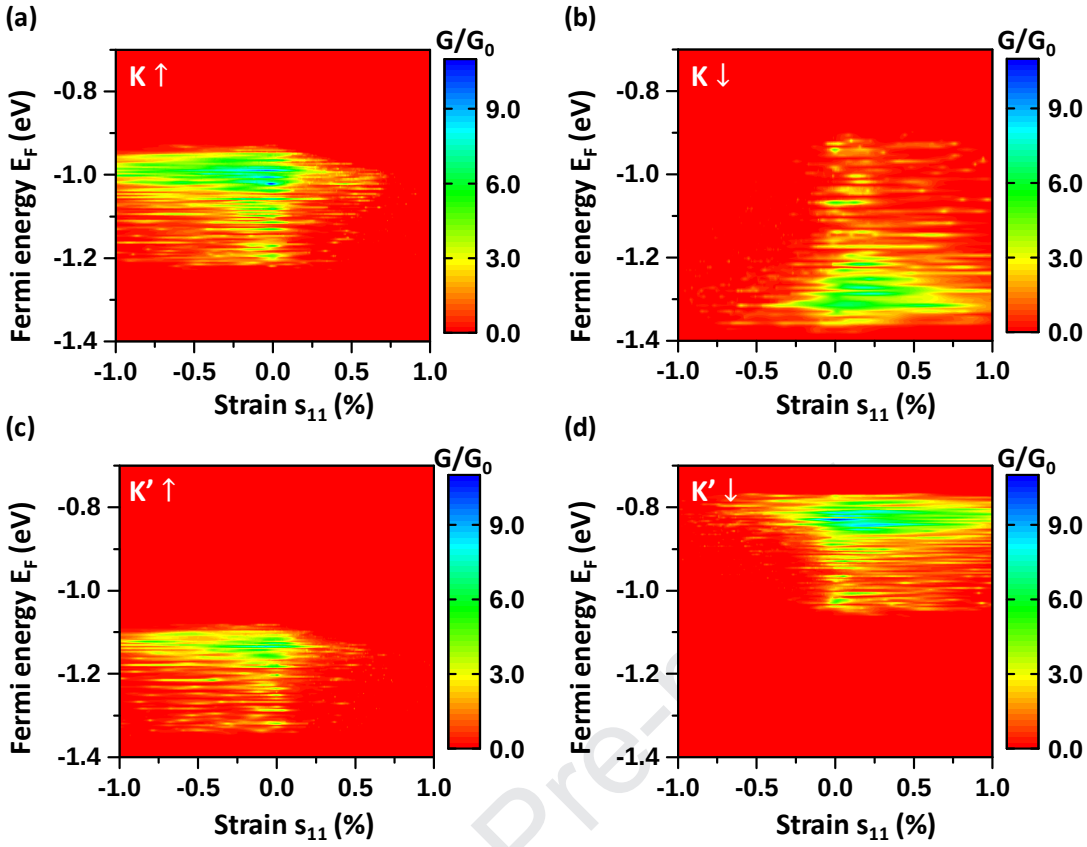

Figure 4

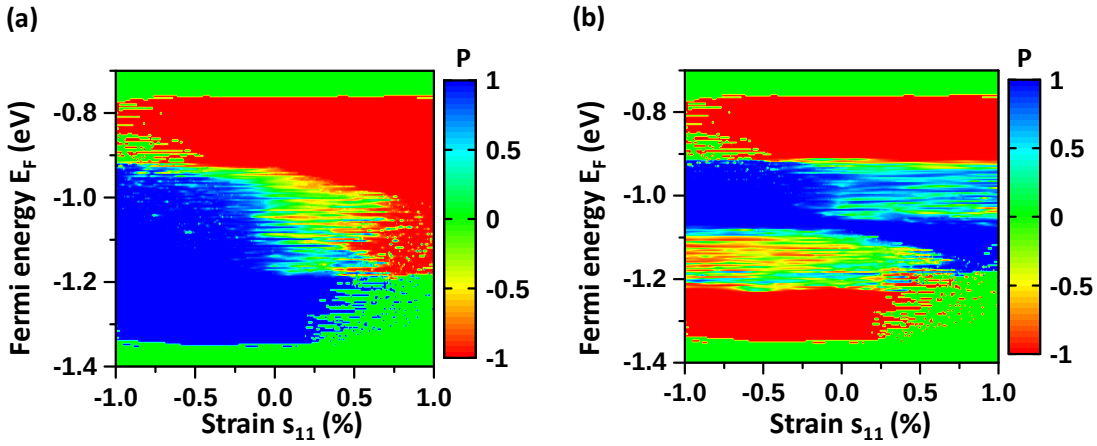

Figure 5

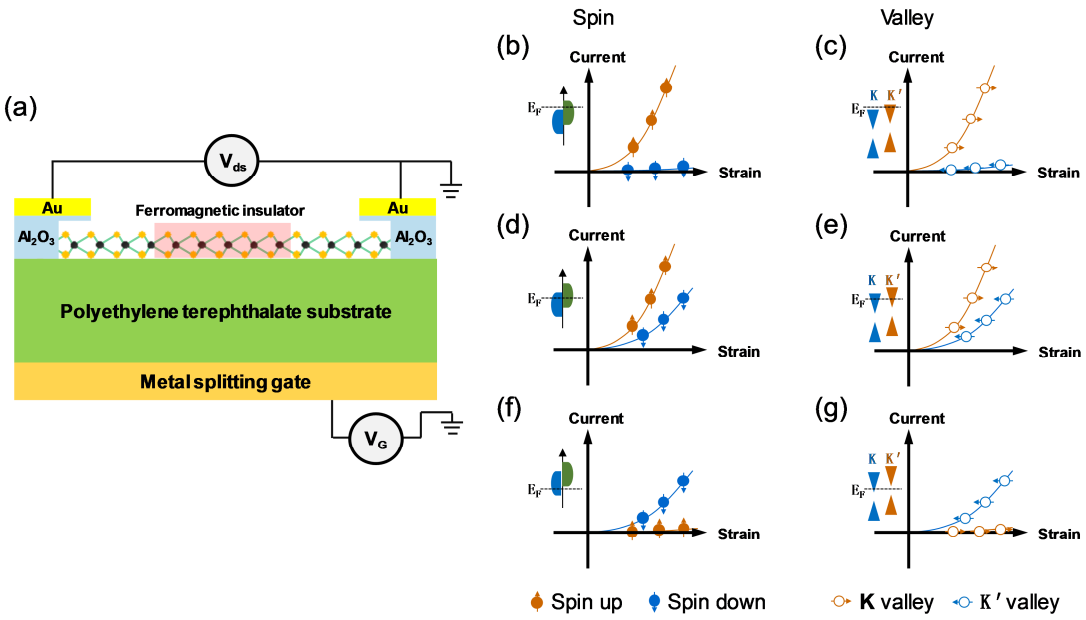

Figure 6

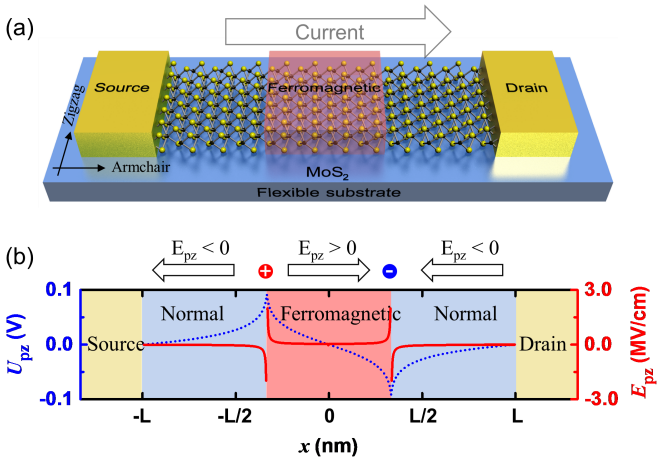

Figure 1

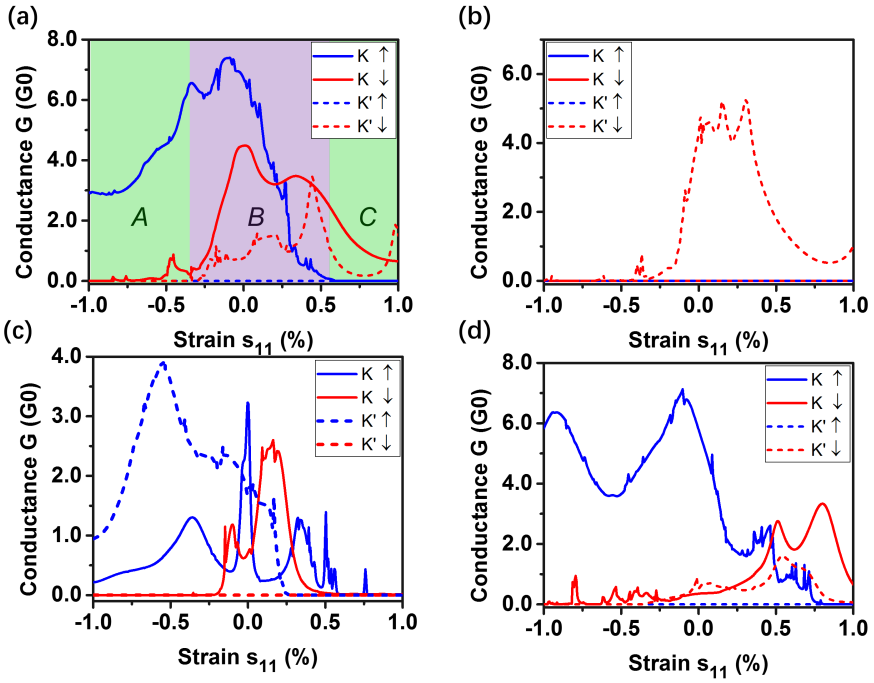

Figure 2

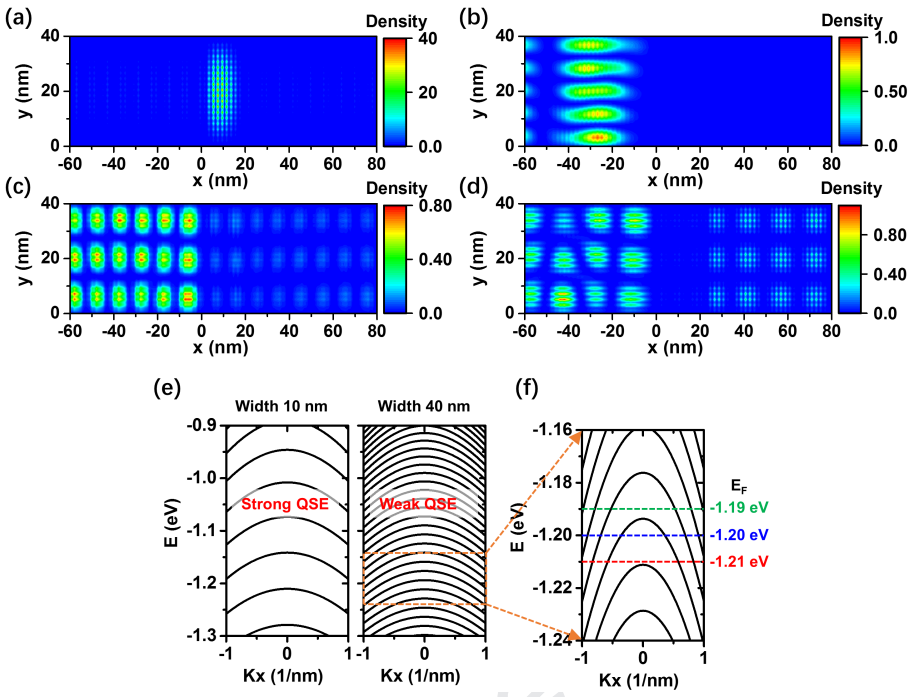

Figure 3

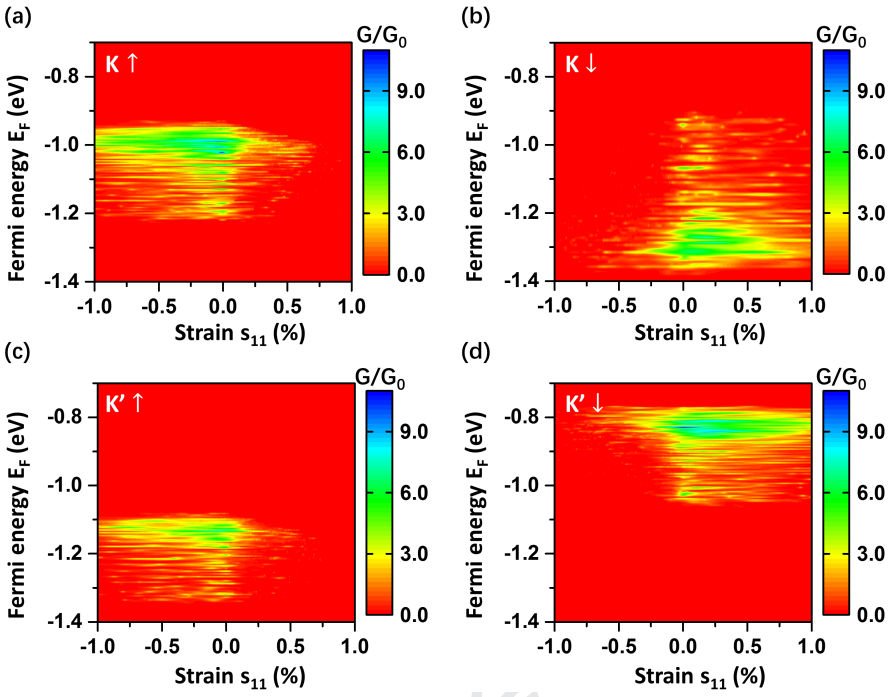

Figure 4

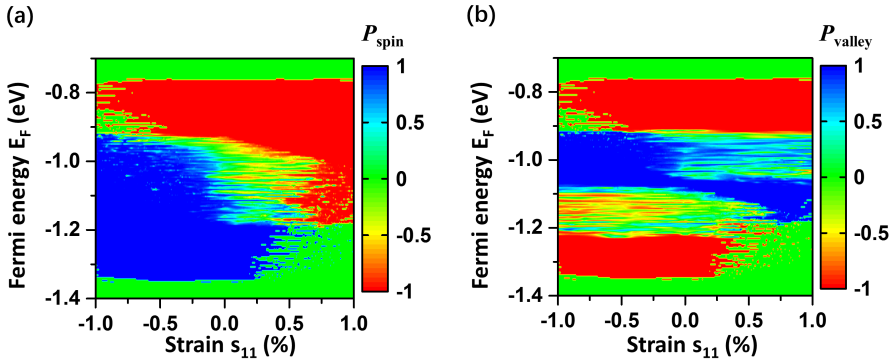

Figure 5

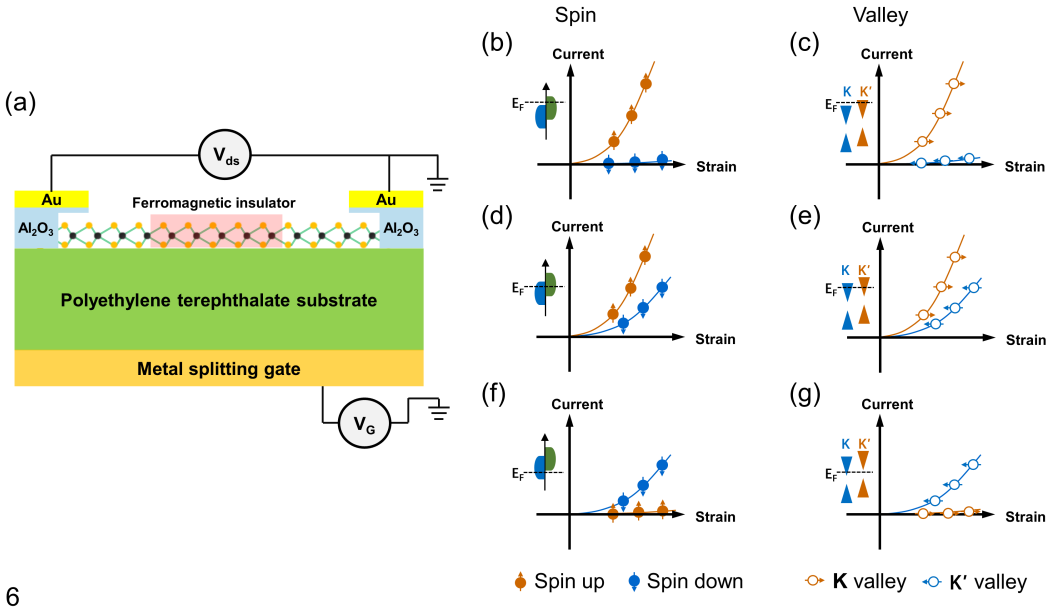

Figure 6

Highlight:

1. Piezotronic effect is used to modulate quantum transport in a normal-ferromagnetic-normal single-layered MoS_2 transistor.
2. Strain-induced piezoelectric field can induce fully spin and valley polarization.
3. Piezotronic effect offer an effective way to design spin and valley filters for quantum information and storage.

Credit Author Statement

Ruhao Liu: Conceptualization, Methodology, Formal analysis, Writing- Original draft preparation; **Gongwei Hu:** Conceptualization, Formal analysis, Validation, Writing- Original draft preparation; **Minjiang Dan:** Formal analysis, Validation; **Yaming Zhang:** Formal analysis, Validation; **Lijie Li:** Writing- Reviewing and Editing; **Yan Zhang:** Supervision, Conceptualization, Methodology, Formal analysis, Writing- Reviewing and Editing

Declaration of interests

☒ The authors declare that they have no known competing financial interests or personal relationships that could have appeared to influence the work reported in this paper.

☐The authors declare the following financial interests/personal relationships which may be considered as potential competing interests: